V International Conference on Adaptive Modeling and Simulation
ADMOS 2011
D. Aubry, and P. Díez (Eds)

MODELING OF PULSED LASER ACTION ON METALS USING DYNAMICALLY ADAPTING GRIDS

VLADIMIR I.MAZHUKIN, ALEXANDR V. MAZHUKIN, MIHAEL M.DEMIN

M.V. Keldysh Institute for Applied Mathematics of RAS
4a Miusskaya sqr.
125047 Moscow, Russia
e-mail: vim@modhef.ru

Key words: Dynamic Grid Adaptation, arbitrary non-stationary coordinate system, transformation function, finite-difference schemes, Phase Transitions, metastable state.

Abstract. Pulsed laser action is characterized by the appearance of the fast phase transitions of the first order which velocity increases as the pulse duration decreases and the intensity increases. Mathematical modeling of the fast phase transitions requires explicit tracking of the interphase boundaries and is a difficult but solvable problem using the method of dynamic adaptation. The method is based on a transition to an arbitrary non-stationary coordinate system allowing obtaining fixed grids with non-moving boundaries in the computational space while its images in the physical space are moving. High velocity of the phase fronts determine the high degree of non-equilibrium of the process exhibiting itself in the appearance of metastable highly overheated states in the solid and liquid phases. Mathematical modeling with explicit front tracking allowed us to determine typical values of overheating (relative to the equilibrium temperature of melting and evaporation) of the solid and liquid phases for different duration of the laser pulse.

1. INTRODUCTION

Pulsed laser ablation which is material removal as a result of irradiation of the target by intense laser pulses is a widely used technology in many applications[1], such as cutting, deposition of thin films, drilling, cleaning, surface microstructuring, etc. This is also an effective method of the controlled production of nano-particles[2]. Furthermore, pulses with very short duration such as pico- or femtosecond are preferable in many applications[3]. In particular, short duration limits thermal diffusion and results in high quality processing.

Despite of the fact that pico-and femtosecond laser ablation became one of the most intensively investigated domains in the laser-matter interaction, the main mechanisms of ablation remain unclear. Usage of ultrashort $\tau_\ell \approx 10^{-12} \div 10^{-15} s$ high-power $G \sim 10^{12} \div 10^{18} W/cm^2$ laser pulses for the material treatment creates unique physical conditions where the duration of the action is comparable with the characteristic time of the thermalization and phase change in the matter. This results in the necessity to consider complex fundamental problems among which are investigation of highly non-equilibrium heating of matter by laser radiation and dynamics of fast phase transitions. But since pico-and femtosecond ablation takes place in very short time and space scale where experimental approaches are very limited, the methods of mathematical modeling become the main investigation tool.

The main peculiarities of the ultrashort laser action on metals are associated with the high rate and volume type of the laser energy deposition. The high heating rate of the condensed phase is connected with the fast phase transformations of matter that are characterized by the transfer of the strong matter and energy flows over the phase boundaries. The speed of the phase fronts reaches or becomes comparable to the one of sound in the condensed media resulting in the formation of the shock waves in solid. The energy transport by the material flow together with the volume type of the energy deposition contribute to the heating of the interphase boundaries to the temperatures significantly higher than the equilibrium melting and evaporation temperature[4]. The mathematical description of these processes if performed within the approximation of different types of Stephan problem[5], which main peculiarity is the presence of moving interphase boundaries with explicit tracking that make the problem non-linear in principal.

The aim of this work is to present the abilities of the dynamic adaptation method that is used to solve the non-equilibrium hydrodynamic type of Stephan problem describing the action of a picosecond laser pulse on the Aluminum target.

2. THEORETICAL MODEL.

The laser radiation propagates from the right to the left and is partially absorbed at the surface of the metal target. Fig.1 shows spatial configuration of the phase fronts $\Gamma_{sl}(t), \Gamma_{lv}(t)$ and the shock wave in the condensed media $\Gamma_{sh,s}(t)$. The statement of the problem includes the following limitations and suppositions.

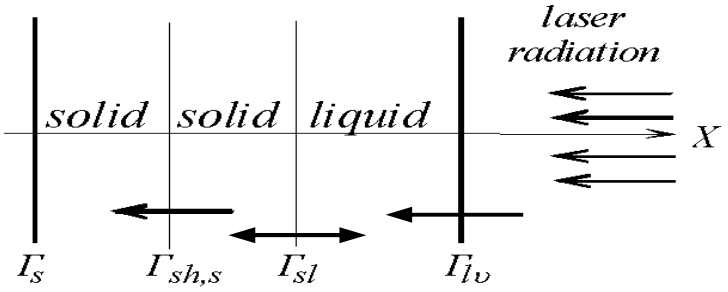

Figure 1: Spatial phase configuration.

The mechanisms of the volume melting and evaporation are not included in the consideration. It is supposed that the melting front appear at the irradiated surface when the temperature reaches T_{m0} and overheated metastable states behave in a stable way during the consideration.

The mathematical description and modeling of the femtosecond laser ablation of hard Aluminum target in vacuum is performed within the framework of a non-equilibrium Stephan-type hydrodynamic and two-temperature and spatially one-dimensional model with multiple fronts written for two media: solid and liquid:

$$\left.\begin{array}{l} \dfrac{\partial\rho}{\partial t}+\dfrac{\partial(\rho u)}{\partial x}=0 \\ \dfrac{\partial(\rho u)}{\partial t}+\dfrac{\partial\left(\rho u^2\right)}{\partial x}=-\dfrac{\partial P}{\partial x} \\ \dfrac{\partial\left(\rho_e\varepsilon_e\right)}{\partial t}+\dfrac{\partial\left(\rho_e u\varepsilon_e\right)}{\partial x}=-\left(P\dfrac{\partial u}{\partial x}+\dfrac{\partial W_e}{\partial x}+g(T_e)(T_e-T_{ph})+\dfrac{\partial G}{\partial x}\right) \\ \dfrac{\partial\left(\rho\varepsilon_{ph}\right)}{\partial t}+\dfrac{\partial(\rho u\varepsilon_{ph})}{\partial x}=-\left(P\dfrac{\partial u}{\partial x}+\dfrac{\partial W_{ph}}{\partial x}-g(T_e)(T_e-T_{ph})\right) \\ \dfrac{\partial G}{\partial x}+\alpha\left(T_e\right)G=0, \qquad \rho_e=z\dfrac{m}{M}\rho, \end{array}\right)_k , \tag{1}$$

$$t>0, \Gamma_s<x<\Gamma_{sh,s}(t)\cup\Gamma_{sh,s}(t)<x<\Gamma_{s\ell}(t)\cup\Gamma_{s\ell}(t)<x<\Gamma_{\ell\upsilon}(t)$$

where $W_e=-\lambda(T_e,T_{ph})\dfrac{\partial T_e}{\partial x}$, $W_{ph}=-\lambda(T_{ph})\dfrac{\partial T_{ph}}{\partial x}$, $\varepsilon_e=C_{ve}(T_e)T_e$, $\varepsilon_{ph}=C_{vph}(T_{ph})T_{ph}$

$$P(\rho,T)=P(\rho_e,T_e)+P\left(\rho_{ph},T_{ph}\right),$$

Here: ρ, u, ε, T, P are the density, gas-dynamic velocity, internal energy and pressure, $\alpha(T_e), R(T_e)$ are the coefficient of volume absorption and the surface reflectivity, G is the laser radiation density, C_v λ are the heat capacity and the heat conductivity coefficient, $g(T_e)$ is the electron-phonon coupling constant. The indexes s, l, υ represent solid, liquid and vapor phases, e, ph represent electron and phonon gas, $k=s,l$

The model of the surface non-equilibrium melting is formulated at the boundary $x=\Gamma_{s\ell}(t)$ as a set of three conservation laws: mass $j^m_{s\ell}$, momentum $j^i_{s\ell}$, energy $j^e_{s\ell}$ and an additional condition for temperature.

All relations are written in the coordinate system moving with the velocity of the solid phase u_s. The velocity of the phase front is given as $\upsilon_{sl}=\upsilon^*_{sl}-u_s$, where υ^*_{sl} is the velocity of the melting-crystallization front in the stationary (laboratory) coordinate system.

$$j^m_{s\ell}=\rho_s\upsilon_{s\ell}=\rho_\ell\left(u_s-u_\ell+\upsilon_{s\ell}\right), \tag{2}$$

$$j^i_{s\ell}=P_s+\rho_s\upsilon^2_{s\ell}=p_\ell+\rho_\ell\left(u_s-u_\ell+\upsilon_{s\ell}\right)^2, \tag{3}$$

$$j^e_{s\ell} = -j^T_s + j^m_{s\ell}\left[H_s + \frac{\upsilon^2_{s\ell}}{2}\right] = -j^T_\ell + j^m_{s\ell}\left[H_\ell + \frac{(u_s - u_\ell + \upsilon_{s\ell})^2}{2}\right], \quad (3)$$

where $H_\ell = C_{ps}\Delta T_{s\ell}$, $H_\ell = C_{p\ell}\Delta T_{s\ell} + L_m$, $W_s = -\lambda(T_{ph,s})\frac{\partial T_{ph,s}}{\partial x}$, $W_\ell = -\lambda(T_{ph,\ell})\frac{\partial T_{ph,\ell}}{\partial x}$

Here H_s, H_ℓ, W_ℓ, W_s are the enthalpy and the heat flows in the solid and liquid phases correspondingly.

The energy conservation law for $j^e_{s\ell}$ can be easily transformed into canonical form of the differential Stephan condition:

$$\left(\lambda_{ph}\frac{\partial T_{ph}}{\partial x}\right)_s - \left(\lambda_{ph}\frac{\partial T_{ph}}{\partial x}\right)_\ell = \rho_s L^{ne}_m \upsilon_{s\ell}, \quad (4)$$

where $L^{ne}_m = L_m + \Delta C_{ps\ell}\Delta T_{s\ell} + \frac{\rho_s + \rho_\ell}{\rho_s - \rho_\ell}\frac{(u_s - u_\ell)^2}{2}$, $\Delta C_{ps\ell} = (C_{p\ell} - C_{ps})$, $\Delta T_{s\ell} = (T_m(P_s) - T_m)$,

L^{ne}_m is the non-equilibrium melting heat.

The differential Stephan condition is supplemented by the phenomenological condition of the temperature equity:

$$T_{s\ell} = T_s = T_\ell = T_m(P_s), \quad \text{where } T_m(P_s) = (T_{m,0} + \theta \cdot P_s), \quad (5)$$

where θ is a constant depending on the material, P_s is the pressure on the surface of the solid phase. The pressure dependence of the melting temperature is typical for the fast phase transitions where the velocity of the phase front υ_{sl} is comparable to the velocity if sound in the condensed media.

The following relations are written for the electron component at $x = \Gamma_{sl}(t)$:

$$\left(\lambda_e\frac{\partial T_e}{\partial x}\right)_s = \left(\lambda_e\frac{\partial T_e}{\partial x}\right)_\ell, \qquad T_{e,s} = T_{e,\ell}, \quad (6)$$

The model of surface non-equilibrium evaporation is formulated within the approximation of the Knudsen layer. Three conservation laws are written at the boundary $x = \Gamma_{k\upsilon}(t)$: mass $j^m_{k\upsilon}$, momentum $j^i_{k\upsilon}$, energy $j^e_{k\upsilon}$ and two additional relations, characterizing the degree of non-equilibrium of the phase transition. All relations at the evaporating surface are written in the coordinate system moving with the velocity of the condensed phase $\upsilon_{k\upsilon} = \upsilon^*_{k\upsilon} - u_k$, $\upsilon^*_{k\upsilon}$ is the evaporation front velocity in the stationary (laboratory) coordinate system:

$$j^m_{k\upsilon} = \rho_k \upsilon_{k\upsilon} = \rho_\upsilon(u_k - u_\upsilon + \upsilon_{k\upsilon}), \quad (7)$$

$$j^i_{k\upsilon} = P_k + \rho_k v^2_{k\upsilon} = p_\upsilon + \rho_\upsilon (u_k - u_\upsilon + v_{k\upsilon})^2 \ , \tag{8}$$

$$j^e_{k\upsilon} = -W_k + j^m_{k\upsilon}\left[H_k + \frac{v^2_{k\upsilon}}{2} \right] = -W_\upsilon + j^m_{k\upsilon}\left[H_\upsilon + \frac{(u_k - u_\upsilon + v_{k\upsilon})^2}{2} \right], \tag{9}$$

where $W_k = -\lambda(T_{ph,k})\dfrac{\partial T_{ph,k}}{\partial x}$, $W_\upsilon = -\lambda(T_\upsilon)\dfrac{\partial T_\upsilon}{\partial x}$, $H_k = C_{p\upsilon}(T_{ph,k} - T_b)$, $H_\upsilon = C_{p\upsilon}(T_\upsilon - T_b) + L_\upsilon$.

The conservation law can be finally written as

$$\left(\lambda_{ph} \frac{\partial T_{ph}}{\partial x} \right)_k = \rho_k v_{k\upsilon} L^{ne}_\upsilon, \quad L^{ne}_\upsilon = L_\upsilon(T_{ph,k}) + C_{p\upsilon}(T_b - T_{ph,k}) + \frac{\rho_k + \rho_\upsilon}{\rho_k - \rho_\upsilon} \frac{(u_\ell - u_\upsilon)^2}{2}$$

The values of T_υ, ρ_υ, p_υ are determined from the relations at the non-equilibirum Knudsen layer[6]:

$$\rho_\upsilon = \alpha_\rho(M)\rho_{sat}, \qquad T_\upsilon = \alpha_T(M) T_{ph,k} \ , \tag{10}$$

$$P_{sat}(T_{ph,k}) = P_b \exp\left[\frac{L_\upsilon}{RT_b} \left(\frac{\Delta T_{ph,k}}{T_{ph,k}} \right) \right], \qquad \rho_{sat} = \frac{P_{sat}(T_{ph,k})}{RT_{phk}},$$

where L^{ne}_υ is the non-equilibrium heat of evaporation , α_T , α_ρ are the Crout coefficients, M is the Mach number at the outer side of the Knudsen layer, ρ_{sat}, P_{sat} are the density and pressure of the saturated vapor, P_b, T_b, are the equilibrium boiling pressure and temperature, T_υ, ρ_υ are the vapor temperature and pressure. At M=1: $T_\upsilon = 0.633\ T_\ell$, $\rho_\upsilon = 0.328\ \rho_{sat}$.

The following relations are written for the electron component and the equation of the laser energy transfer at the boundary $x = \Gamma_{\ell\upsilon}(t)$:

$$-\lambda_e \frac{\partial T_e}{\partial x} = \sigma T_e^4, \ G(t) = (1 - R(T_e)) \cdot G_0 \exp\left(-\left(\frac{t}{\tau_L} \right)^2 \right) \tag{11}$$

where σ is the Stephan-Boltzmann constant, R is the surface reflectivity coefficient.

The temperature dependencies of the transport and optical properties $\lambda_e(T_e, T_{ph})$, $\lambda_{ph}(T_{ph})$, $g(T_e)$, $\alpha(T_e)$, $R(T_e)$ were determined using the approach from Refs.[7,8].

3. THE COMPUTATION ALGORITHM AND DIFFERENTIAL SCHEMES.

The main peculiarity of the Stephan problems is the presence of the boundaries moving with the velocities $v_{s\ell}$ and $v_{k\upsilon}$. That means that the problem (1) – (11) will be non-linear even with constant values of the optical and thermophysical properties. The presence of the moving boundaries also results in significant complication of the computational algorithm. At

the low rate of the phase transformations (the velocity of the phase front is much lower than the speed of sound), the processes of the phase transformation take place in a quasi-equilibrium way. The interphase boundaries in these cases are not tracked explicitly. The account of the phase transformations is performed using so-called enthalpy approach[9], where the smoothing function is used instead of the differential Stephan condition. In this case the phase transformation is taken into account using a singular additive to the heat capacity (to the equation of state) in the point of the phase transition. The fast phase transitions (the transition velocity is comparable to the one of sound in the condensed media) that are typical for powerful pulsed laser action take place in the conditions of high non-equilibrium caused by the rapid material flow[10] over the interphase boundary. The enthalpy approach is not applicable in these situations since the smoothing of the heat capacity function narrows the class of solutions of the phase transformations in the media, in particular, it excludes from the consideration the phenomena of overheating and overcooling of the condensed media. The interphase boundaries should be explicitly tracked in order to take these phenomena into account.

The method of dynamic adaptation[11,12] is used to solve the non-linear system (1)-(11) within the domain with the moving boundaries $\Gamma_{sl}(t)$, $\Gamma_{kv}(t)$ and $\Gamma_{sh,s}(t)$. This method is based on a transition to an arbitrary non-stationary coordinate system.

The transition to an arbitrary non-stationary coordinate system is performed using an automatic coordinate transformation using the sought solution. The transition is performed from the physical space $\Omega_{x,t}$ with Euler variables (x,t) into the computational space with non-stationary coordinate system $\Omega_{q,\tau}$ and variables (q,τ):

$$\left\{\begin{array}{l}
\dfrac{\partial}{\partial\tau}(\psi\rho)+\dfrac{\partial}{\partial q}(\rho(u+Q))=0,\\
\dfrac{\partial}{\partial\tau}(\psi\rho u)+\dfrac{\partial}{\partial q}(P+\rho u(u+Q))=0,\\
\dfrac{\partial}{\partial\tau}(\psi\rho_e\varepsilon_e)+\dfrac{\partial}{\partial q}(\varepsilon_e\rho_e(u+Q))=-P\dfrac{\partial u}{\partial q}-\dfrac{\partial W_e}{\partial q}-\psi g(T_e)(T_e-T_{ph})-\dfrac{\partial G}{\partial q},\\
\dfrac{\partial(\rho\varepsilon_{ph})}{\partial\tau}+\dfrac{\partial}{\partial q}(\varepsilon_{ph}\rho(u+Q))=-P\dfrac{\partial u}{\partial q}-\dfrac{\partial W_{ph}}{\partial q}+\psi g(T_e)(T_e-T_{ph}),\\
\dfrac{\partial G}{\partial q}+\psi\kappa(\rho,T)G=0,\\
\dfrac{\partial\psi}{\partial\tau}=-\dfrac{\partial Q}{\partial q},\qquad \psi=\dfrac{\partial x}{\partial q}
\end{array}\right\} \tag{12}$$

$\tau>\tau_0$, $\Gamma_s<q<\Gamma_{sh,s}\cup\Gamma_{sh,s}<q<\Gamma_{s\ell}\cup\Gamma_{s\ell}<q<\Gamma_{\ell v}$

The initial differential system (1) is transformed into the extended system (12) during this transition to an arbitrary non-stationary coordinate system. Here the first five equations describe the physical processes and the last one is the equation of the reverse transformation

which type, properties and boundary conditions depend on the particular form of the transformation function Q. The transformation function can be assumed to be the mass flow $Q=-\rho u$. This equation is then used to construct the grid dynamically adapting to the solution. Its difference analogue describes the grid nodes dynamics and the function Q performs controlled motion of the grid nodes adapted to the dynamics of the sought solution.

The transformation functions Q are determined from the quasi-stationarity principle that states that it is necessary to determine the system where all processes take place is a stationary way. In this problem, two energy equations were used to determine the function Q from the condition $\frac{\partial \varepsilon_e}{\partial \tau} = \frac{\partial \varepsilon_{ph}}{\partial \tau} = 0.$

Initial and boundary conditions for the system (12) are formulated in the following way.

$$\tau = \tau_0: \qquad T_e(\tau_0, q) = T_{ph}(\tau_0, q) = T_0, \qquad \psi(\tau_0, q) = 1,$$

$$q = q_0: \qquad -\frac{\lambda_e \rho}{\psi}\frac{\partial T_e}{\partial q} = -\frac{\lambda_{ph}\rho}{\psi}\frac{\partial T_{ph}}{\partial q} = 0, \qquad Q_{s\ell}(\tau, q_0) = 0$$

$$q = \Gamma_{s\ell}: \qquad \left(\frac{\lambda_e \rho}{\psi}\frac{\partial T_e}{\partial x}\right)_s = \left(\frac{\lambda_e \rho}{\psi}\frac{\partial T_e}{\partial x}\right)_\ell, \qquad T_{sl} = T_{ph,s} = T_{ph,l} = T_m$$

$$Q_{s\ell} = -\rho_s \upsilon_{s\ell}, \quad Q_{s\ell} = \left[\left(\frac{\lambda_{ph}\rho}{\psi}\frac{\partial T_{ph}}{\partial x}\right)_s - \left(\frac{\lambda_{ph}\rho}{\psi}\frac{\partial T_{ph}}{\partial x}\right)_\ell\right] L_m^{-1}, \quad \upsilon_{s\ell} = -\rho_s^{-1} Q_{s\ell}$$

$$q = \Gamma_{k\upsilon}: \qquad \left(-\frac{\lambda_{ph}\rho}{\psi}\frac{\partial T_{ph}}{\partial q}\right)_k = -L_\upsilon Q_{k\upsilon}, \qquad Q_{k\upsilon} = -\rho_k \upsilon_{k\upsilon} \tag{13}$$

$$Q_{k\upsilon} = -\rho_\upsilon(\upsilon_{k\upsilon} - u), \quad P_k + Q_{k\upsilon}\upsilon_{k\upsilon} = p_\upsilon - \rho_k(\upsilon_{k\upsilon} - u)^2, \quad T_\upsilon = \alpha_T(M)T_{ph,k}, \quad \rho_\upsilon = \alpha_\rho(M)\rho_H,$$

$$\left(\frac{\lambda_e \rho_e}{\psi}\frac{\partial T_e}{\partial q} = \sigma T_e^4, \quad G(\tau) = A(\hbar\omega, T_e)\cdot G_0 \exp\left(-\left(\frac{\tau}{\tau_L}\right)^2\right)\right)_k \qquad \text{k=s,l}$$

The differential problem (12), (13) is approximated by a set of conservative difference schemes written on the computational grids for each sub-domain (solid and liquid). The solution of the obtained non-linear differential equations was performed using enclosed iterative procedures.

4. RESULTS OF THE MODELING

The surface of the Aluminum target in vacuum is irradiated by a laser pulse with Gaussian time distribution of intensity $G(t) = (1 - R(\hbar\omega, T_e))\cdot G_0 \exp\left(-\left(\frac{\tau}{\tau_L}\right)^2\right)$, duration of $\tau_L = 10^{-12}\, s$, wavelength $\lambda = 0.8\,\mu m$, fluence of $F = 0.5\, J\, cm^{-2}$ and peak intensity of $G_0 = \frac{F}{\pi^{1/2}\tau_L} = 2.82\cdot 10^{11}\, W\, cm^{-2}$.

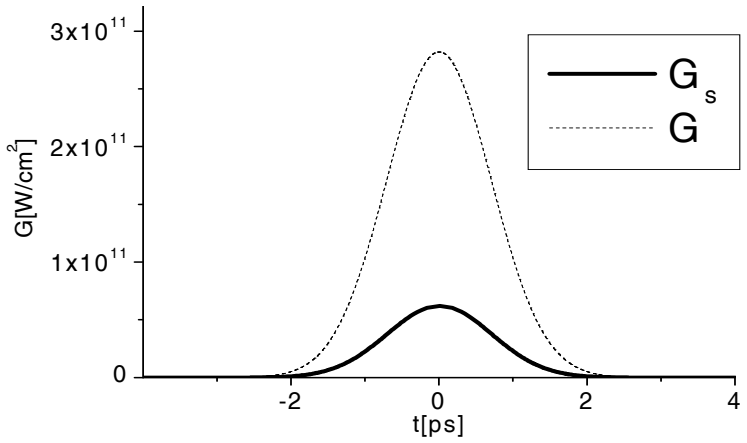

Figure 2: Time profile of the initial laser $G(t)$ and absorbed $G_s(t)$ intensity.

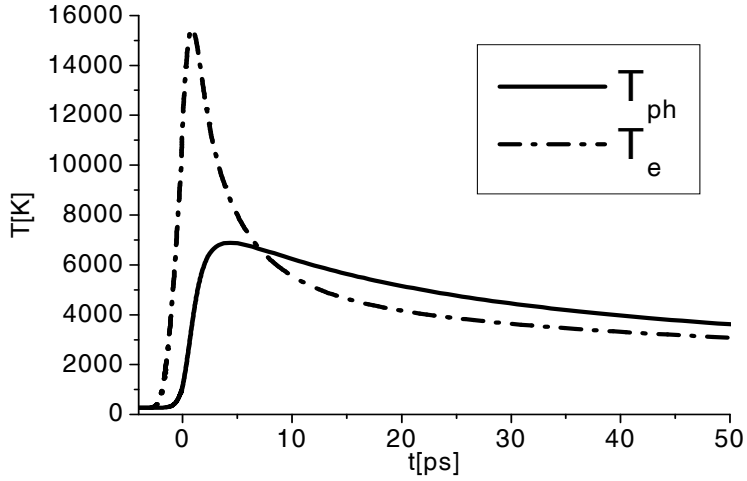

Figure 3: Time profile of the surface temperatures $T_e(t)$, $T_{ph}(t)$.

The absorbed portion of the radiation $G_s(t) = (1 - R(\hbar\omega, T_e)) \cdot G(t)$, Fig.2, is completely released in the electron component. Due to the low heat capacity of electron and slow energy exchange between the subsystems, the electron gas is rapidly heated to the temperatures significantly higher than the one on the lattice $T_e >> T_{ph}$. Fig.3 shows the time dependence of the temperatures $T_e(t), T_{ph}(t)$ at the surface. The maximum value of the electron temperature $T_{e\,\max}(t) \approx 1.55 \cdot 10^4 K$ is reached right after the peak intensity. The maximum separation of the temperatures $\Delta T(t) = T_e(t) - T_{ph}(t)$ reaches the value of $1.2 \cdot 10^4 K$, Fig. 4. The rapid rise of the electron temperature results in the rise of the energy exchange coefficients $g(t)$ and $\lambda_e(t)$, Fig.5. The coupling factor $g(t)$ is increased by more than 1.5 orders, resulting in the fast rise of the lattice temperature and decrease of the electron one. The maximum value of

the lattice temperature $T_{ph,\max}^{\mathrm{Al}} \approx 7 \cdot 10^3 K$ are reached after the end of the laser pulse at the end of the non-equilibrium period at $t \approx 7.5\ ps$. The significant increase of the electron heat conductivity coefficient $\lambda_e(t)$, approximately by ~ 10 times results in the sharp rise of the energy carry-out from the heating zone by the heat conductivity so that the value of $\Delta T(t) < 0$ becomes negative, $T_e < T_{ph} \approx 10^3 K$, Fig.4. The complete temperature equilibration takes place at about $t \approx 60\ ps$.

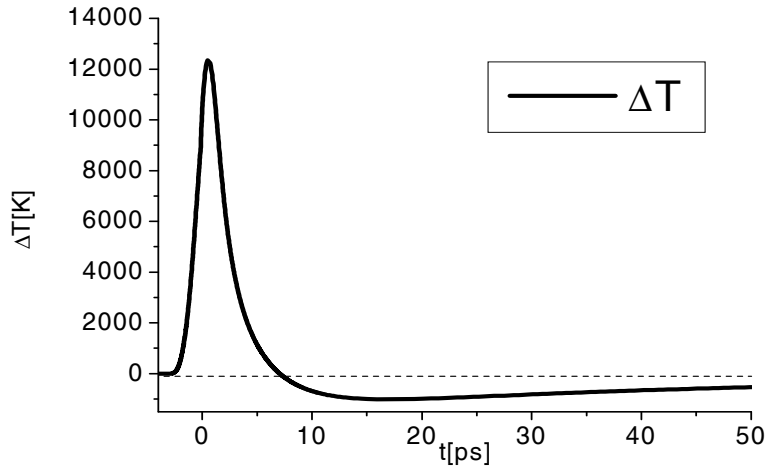

Figure 4: Time profile of the temperature difference $\Delta T(t) = T_e(t) - T_{ph}(t)$.

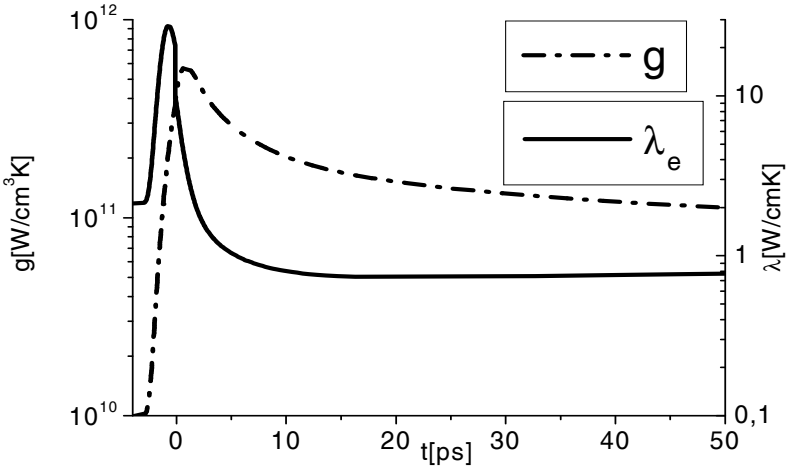

Figure 5: Time profile of the coupling constant $g(t)$ and the electron heat conductivity $\lambda_e(t)$.

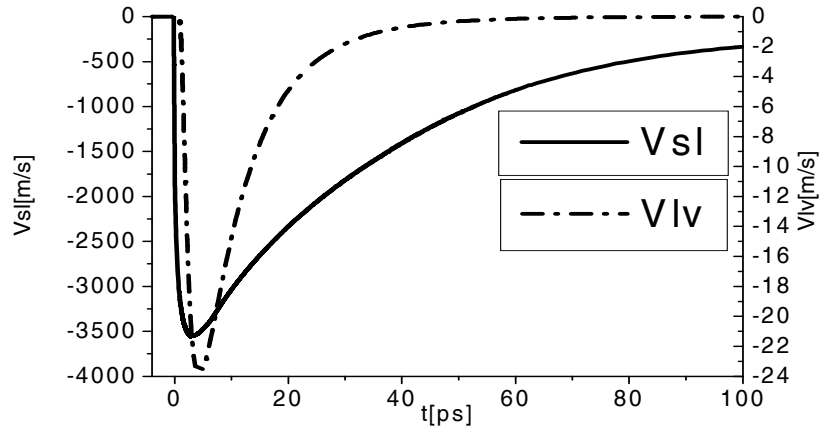

Figure 6: Time profile of the melting $v_{s\ell}(t)$ and evaporation $v_{\ell v}(t)$ velocity.

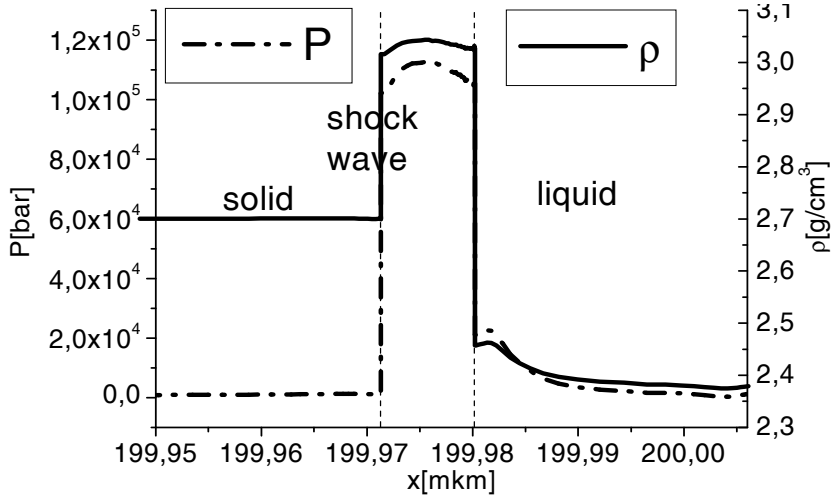

Figure 7: Spatial profiles of the pressure $P(x)$ and density $\rho(x)$.

The main peculiarity of the picosecond action is the high rate of the laser energy release that causes the high rates of the target heating and the phase transformations. Fig.6 shows the time dependencies of the propagation velocities of the melting $v_{s\ell}(t)$ and evaporation $v_{\ell v}(t)$ fronts. Their maximum values are 3.5 km/s and 24 m/s correspondingly. The velocity of the melting front becomes comparable to the velocity of sound in the solid phase generating the pressure of $P_s \approx 0.11$ Mbar at the melting surface that is enough to generate a compression wave in solid that is then transformed into a shock wave, Fig.7. The high velocities of the phase fronts provide high material and energy flows over the interphase boundaries. Together with the volume heating of the lattice, that causes interesting physical phenomena – overheating of the solid and liquid surface and formation of the sub-surface temperature maximums, Fig.8. According to the computations, the overheated metastable states in the solid and liquid

phases can exceed the equilibrium values of the melting T_m and evaporation T_b temperatures by several thousands of degrees.

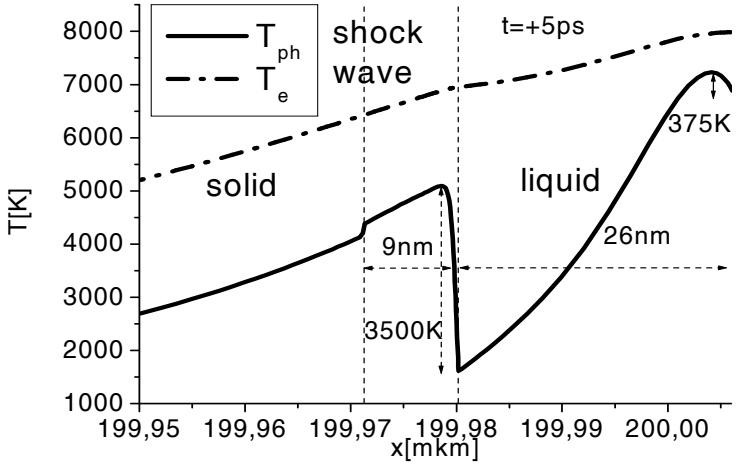

Figure 8: Spatial profiles of the temperatures $T_e(x)$, $T_{ph}(x)$ at $t = 5\,ps$.

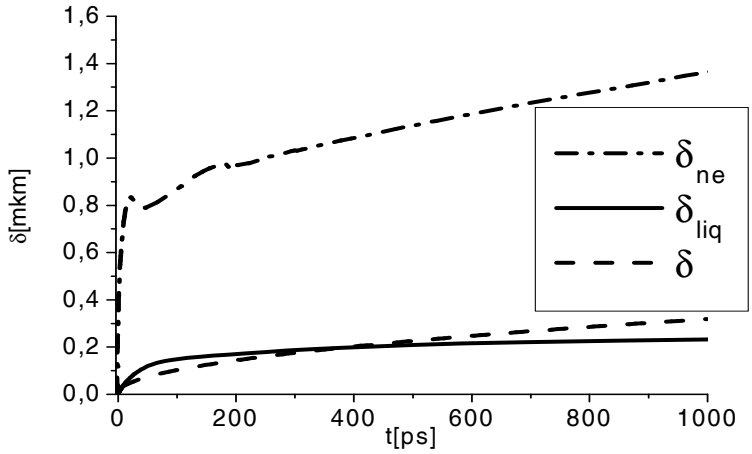

Figure 9: Time profiles of non-equilibrium $\delta_{ne}(t)$ and equilibrium $\delta(t)$ heating zones and thickness of liquid $\delta_{liq}(t)$

Another manifestation of the non-equilibrium effects is very large size of the heat action zone that is determined by the heat conductivity of electron Fermi-gas. Fig. 9 compares the non-equilibrium heating zone $\delta_{ne}(t)$ and the equilibrium one $\delta(t)$ that is determined as $\delta(t) = (\lambda / C_p\, t)^{1/2}$. Their relation $\delta_{ne}(t)/\delta(t) \approx 7 \div 10$ shows how much the non-equilibirum zone is larger that the equilibrium one.

5. CONCLUSION

The mathematical modeling of ultrashort laser action on solid target was performed. The behavior of the main processes under the conditions of non-equilibrium heating was analyzed. The most important point in this investigation is the usage of the method of dynamic adaptation allowing explicit tracking interphase boundaries and fronts of the shock waves. Their tracking allows obtaining results that are not reachable using other solution methods. In particular, the dynamic adaptation allowed to investigate the dynamics of the fast phase fronts and associated highly overheated metastable states in solid and liquid phases appearing during fast energy release in the condensed media.

The work was supported by RFBR (projects No 10-07-00246-a, No 09-07-00225-a).

REFERENCES.

1. Bauërle D., *Laser Processing and Chemistry*_Springer-Verlag, Berlin (2000).
2. Mene´ndez -Manjo´n A., Barcikowski S., Shafeev G.A., Mazhukin V.I., Chichkov B.N. Influence of beam intensity profile on the aerodynamic particle size distributions generated by femtosecond laser ablation. *Laser and Particle Beams*(2010) **28**:45–52.
3. von der Linde D., Sokolowski-Tinten K. The physical mechanisms of short-pulse laser ablation. Appl. Surf. Sci.(2000) **154-155**:1-6.
4. Mazhukin V.I., Lobok M.G., Chichkov B.N.. Modeling of fast phase transitions dynamics in metal target irradiated by pico and femto second pulsed laser. Applied Surface Science. (2009)**255**:5112-5115.
5. Mazhukin V.I., Samarskii A.A. Mathematical Modeling in the Technology of Laser Treatments of Materials. Review. Surveys on Mathematics for Industry, (1994) **4**:85-149.
6. Mazhukin V.I., Prudkovskii P.A., Samohin A.A.. On gas-dynamic boundary conditions at the evaporation front. *Matematicheskoe modelirovanie*(1993) **5**:3-10.
7. Mazhukin V.I., Mazhukin A.V., Koroleva O.N.. Optical properties of electron Fermi-gas of metals at arbitrary temperature and frequency. *Laser Physics* (2009)**19**:1179 - 1186
8. Mazhukin A.V., Mazhukin V.I., Demin M.M. Modeling of femtosecond laser ablation of Al film by laser pulses. *Applied Surface Science* (2011)**257**:5443–5446.
9. Samarskii A.A., Moiseenko B.D.. Economical scheme of through-calculation for multidimensional Stephan problem. *Zhurnal Vychislitel'noi matematiki i vychislitel'noi fiziki* (1965) **5**:816-827.
10. Mazhukin V.I., Smurov I., Flamant G. Overheated Metastable States in Pulsed Laser Action on Ceramics. *J. Applied Physics* (1995)**78**:1259-1270.
11. Mazhukin V.I., Smurov I., Dupuy C., Jeandel D. Simulation of Laser Induced Melting and Evaporation Processes in Superconducting. *J. Numerical Heat Transfer Part A*(1994)**26**: 587-600.
12. Breslavskii P. V. and Mazhukin V. I. Dynamic Adaptation Method in Gasdynamic Simulations with Nonlinear Heat Conduction. *Computational Mathematics and Mathematical Physics* (2008)**48:**2102–2115.